ARTICLE

Self-Ordered Anodic Aluminum Oxide Formed by H_2SO_4 Hard Anodization

Kathrin Schwirn, Woo Lee,* Reinald Hillebrand, Martin Steinhart, Kornelius Nielsch, and Ulrich Gösele

Max Planck Institute of Microstructure Physics, Weinberg 2, D-06120 Halle, Germany

ABSTRACT The self-ordering of nanoporous anodic aluminum oxide (AAO) in the course of the hard anodization (HA) of aluminum in sulfuric acid (H_2SO_4) solutions at anodization voltages ranging from 27 to 80 V was investigated. Direct H_2SO_4-HA yielded AAOs with hexagonal pore arrays having interpore distances D_{int} ranging from 72 to 145 nm. However, the AAOs were mechanically unstable and cracks formed along the cell boundaries. Therefore, we modified the anodization procedure previously employed for oxalic acid HA ($H_2C_2O_4$-HA) to suppress the development of cracks and to fabricate mechanically robust AAO films with D_{int} values ranging from 78 to 114 nm. Image analyses based on scanning electron micrographs revealed that at a given anodization voltage the self-ordering of nanopores as well as D_{int} depend on the current density (*i.e.*, the electric field strength at the bottoms of the pores). Moreover, periodic oscillations of the pore diameter formed at anodization voltages in the range from 27 to 32 V, which are reminiscent of structures originating from the spontaneous growth of periodic fluctuations, such as topologies resulting from Rayleigh instabilities.

KEYWORDS: anodic aluminum oxide · self-assembly · nanopores · membranes · hard anodization · templates · modulated pore structure

Self-ordered nanoporous anodic aluminum oxide (AAO) is a versatile platform for applications in the fields of sensing, storage, separation, and the synthesis of one-dimensional nanostructures.[1–9] In contrast to mesoporous materials formed by the self-assembly of surfactants and block copolymers, AAOs consist of arrays of nanopores with high aspect ratios that may extend several cm^2.[10–12] Self-ordered AAOs are obtained by mild anodization (MA) in three major self-ordering regimes with H_2SO_4, $H_2C_2O_4$, and H_3PO_4 solutions as electrolytes under appropriate electrochemical conditions.[13–18] The MA process, however, requires an anodization time of typically more than 2 days, and self-ordered pore growth only occurs in narrow process windows. Various attempts have been made to overcome the drawbacks associated with the MA process.[18–22] A particularly attractive alternative is the hard anodization (HA) of Al substrates typically performed at high anodization voltages U ranging from 40 to 150 V. $H_2C_2O_4$-based HA enables the rapid fabrication of long-range ordered AAOs under self-ordering regimes characterized by interpore distances D_{int} between 200 and 300 nm, a range that is not accessible by conventional MA. Moreover, $H_2C_2O_4$-HA allows the time-consuming two-step procedure required for MA to be circumvented.[22] Nanopores with diameters D_p ranging from 49 to 59 nm and depths T_p ranging from 50 to 70 μm can be grown on a time scale of 1 h and, therefore much faster, than under MA conditions. Another important advantage of the HA process is the accessibility of AAOs with porosities (portion of the pore openings of the membrane surface) three times lower than those of MA membranes.

It is highly desirable to extend the range of accessible D_{int} values for HA AAOs to the 100 nm and sub-100 nm range. Analogous to MA, where the use of H_2SO_4 as an electrolyte leads to smaller D_{int} and D_p values as compared to anodization with $H_2C_2O_4$, H_2SO_4-HA is a promising approach toward the reduction of D_{int} and D_p under HA conditions that yields AAOs with D_{int} values in the range from 57 to 130 nm and D_p values in the range from 22 to 50 nm.[21,23–27] However, the AAO films thus obtained have poor mechanical properties because they exhibit a high density of cracks and structural defects. Therefore, it is necessary to develop a H_2SO_4-HA process that provides AAOs stable enough for real-life applications. To this end, a better understanding of the mechanism of the HA process is required.

Here, we report on the detailed investigation of the self-ordering behavior in nanoporous AAOs during H_2SO_4-HA at U = 27–80 V. Starting from the procedures reported by Chu *et al.* (denoted as **type I HA**), we developed a modified H_2SO_4-HA process that involves less harsh anodization

*Address correspondence to woolee@mpi-halle.de.

Received for review July 31, 2007 and accepted January 10, 2008.

Published online January 26, 2008.
10.1021/nn7001322 CCC: $40.75

conditions (denoted as **type II HA**).[21,22] **Type I HA** starts under galvanostatic conditions (constant current density) and switches to potentiostatic conditions (constant anodization voltage) after having reached a set target voltage U_T. This process leads to the formation of AAO membranes with insufficient mechanical stability. In the case of **type II HA**, potentiostatic conditions are maintained during the entire process by starting the anodization under MA conditions. Subsequently, the anodization voltage is gradually increased, following a properly designed voltage profile. We show that **type II HA** yields AAOs with D_{int} values ranging from 78 to 114 nm and D_p values ranging from 15 to 30 nm that show significantly improved mechanical stability and structural integrity. Furthermore, we report a self-ordering phenomenon that leads to the occurrence of periodic oscillations of the pore diameter in the voltage range from $U = 27$ V to $U = 32$ V, which is, however, not understood in detail yet.

RESULTS AND DISCUSSION

Type I HA. Analyzing the morphologies of AAO layers obtained by stopping **type I HA** performed at $U_T = 40$ V at different stages revealed that the mechanism of the pore formation is different from that in MA. Figure 1 shows typical SEM images of the undersides of AAOs after the opening of the pore bottoms. The obtained morphologies correspond to specific U values in the voltage profile of **type I HA** (Figure 9). If **type I HA** was interrupted at $U = 27$ V, the nanopore arrays were disordered (Figure 1a). However, the nanoporous films exhibited a significantly better ordering at $U = 32$ V (Figure 1b). The ordering further improved until U reached U_T (Figure 1c).

To analyze the pore arrays in more detail, cross-sectional specimens of **type I HA** samples, the anodization of which was stopped at $U = 27$ V (Figure 2a), $U = 32$ V (Figure 2b), and during the transition from the galvanostatic to the potentiostatic mode at $U = U_T = 40$ V (Figure 2c) were investigated by transmission electron microscopy (TEM). In general, independent of the U_T value and for current densities $j < 750$ mA cm^{-2} disordered pore arrays containing some pores with closed ends form at $U \leq 27$ V. In the segments of the pore arrays that were formed at $U = 27$–32 V, where the initially disordered pore growth becomes ordered, periodic oscillations of the pore diameter occur, as discussed below in more detail (Periodic Oscillations of the Pore Diameter). The segments of the AAOs formed at $U > 32$ V are characterized by straight and aligned pores with uniform diameter.

We analyzed scanning electron microscopy (SEM) images of pore arrays corresponding to different stages of **type I HA** by real-space image analysis in order to investigate the evolution of D_{int} quantitatively. Figure 3a displays D_{int} and the proportionality constant $\zeta_{HA} = D_{int}/U$ as a function of U as long as the system is in the galvanostatic regime (voltage range below 40 V in Figure 3a). It is evident that D_{int} increases along with U, for example, from $D_{int} = 55$ nm at $U = 27$ V to $D_{int} = 72$ nm at $U = U_T = 40$ V. In addition, we measured D_{int} for different U_T values at the transition from the galvanostatic to the potentiostatic mode (voltage range above 40 V in Figure 3a). We found a linear dependence of D_{int} on U_T. D_{int} increases from 91 nm at $U_T = 50$ V to 117 nm at $U_T = 65$ to 145 nm at $U_T = 80$ V. Moreover, D_{int} increases slightly without affecting the ordering of the pore arrays as the anodization is continued at U_T in the potentiostatic mode, for example, from 72 nm at the

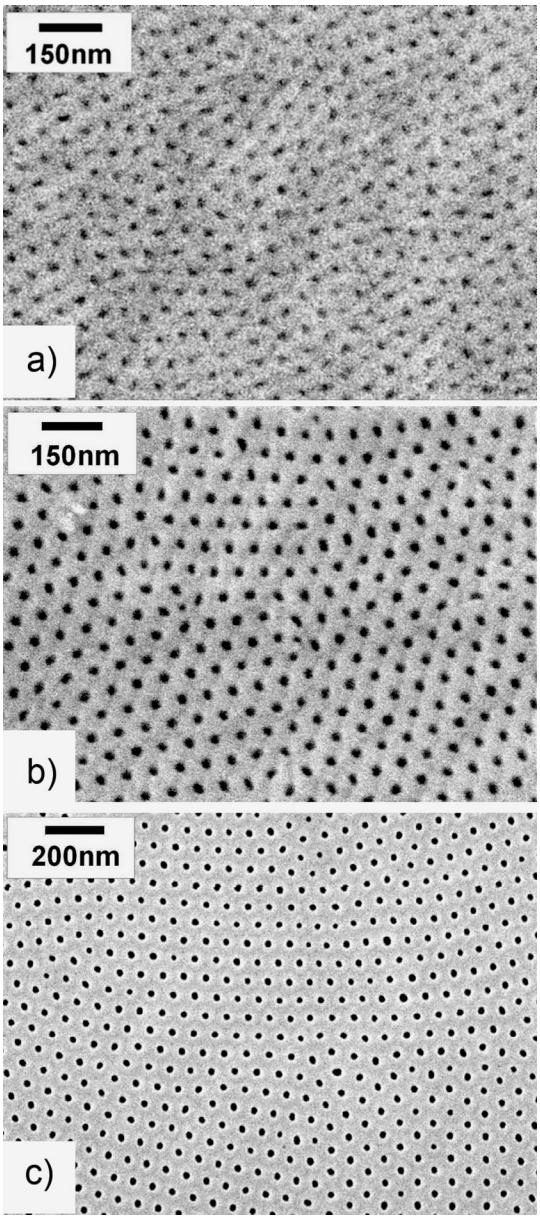

Figure 1. SEM images of the undersides of AAOs formed by type I HA. After selectively etching the Al substrate, the pore bottoms were opened by ion milling. (a, b) AAOs formed under galvanostatic conditions ($j = 120$ mA cm^{-2}). The anodization was stopped at (a) $U = 27$ V and (b) $U = 32$ V. (c) AAO membrane the anodization of which was stopped at the transition point from the galvanostatic mode to the potentiostatic mode with U_T set to 40 V.

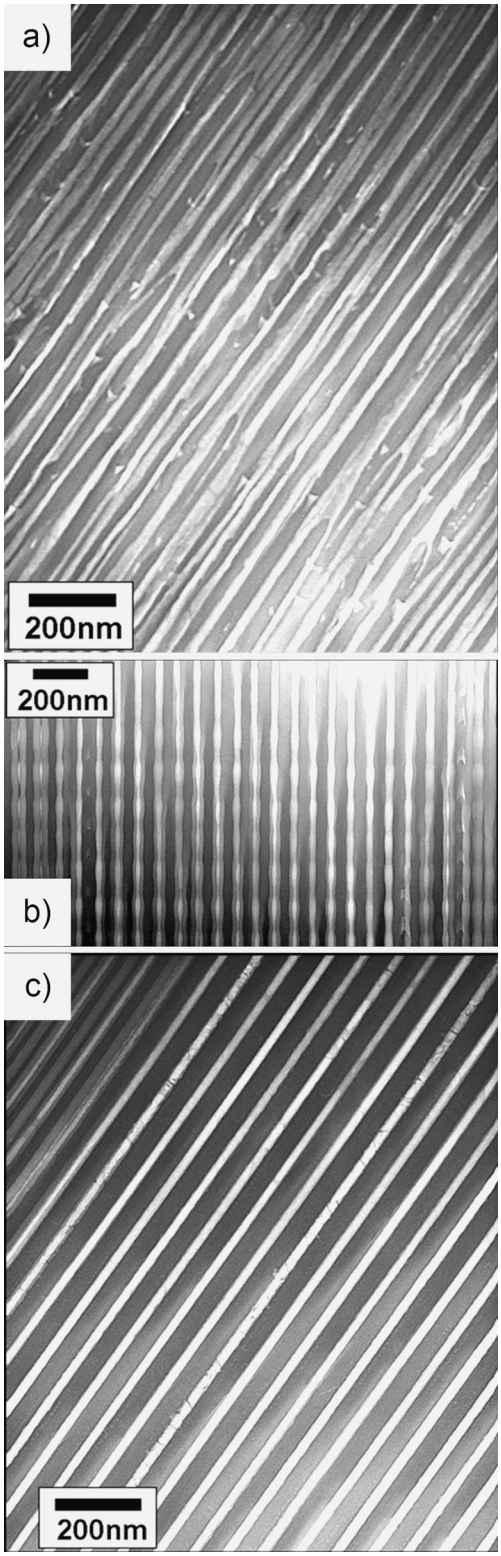

Figure 2. Cross-sectional TEM images of AAOs in the proximity of the pore bottoms formed by type I HA at (a) $U < 27$ V, (b) $U = 27$–32 V, and (c) $U = 32$–40 V under galvanostatic conditions ($j = 120$ mA cm^{-2}).

transition point to 75 nm after further anodization for 10 min at $U_T = 40$V. ζ_{HA} lies in the range from 1.8 to 2.0 nm V^{-1} and is therefore significantly smaller than for MA ($\zeta_{MA} = 2.5$ nm V^{-1}). Under galvanostatic conditions,

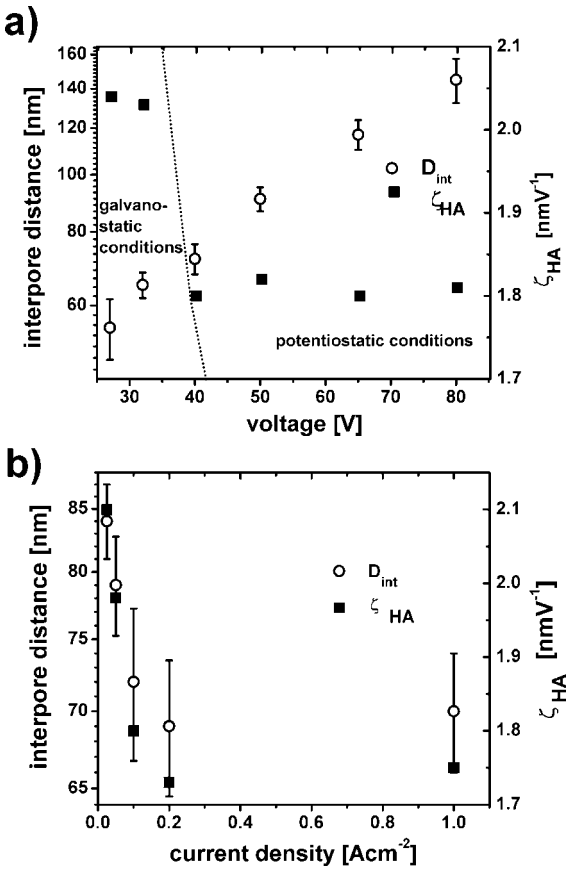

Figure 3. Dependence of D_{int} and ζ_{HA} for type I HA (a) on the anodization voltage and (b) on the current density. The error bars correspond to the full widths at half-maximum of the nearest neighbor peaks in the pair distribution functions obtained from SEM images. In (a) below 40 V the system was in the galvanostatic mode with $j = 120$ mA cm^{-2} and $U_T = 40$ V. In the voltage range from 50 to 80 V D_{int} and ζ_{HA} were determined at the transition point from the galvanostatic to the potentiostatic regime ($U = U_T$) with the current density limitation adjusted to 200 mA cm^{-2}. In (b) different current densities for the galvanostatic regime were set, and D_{int} and ζ_{HA} were determined at the transition point from the galvanostatic to the potentiostatic regime at $U_T = 40$ V.

ζ_{HA} decreases until U equals U_T. The largest domains identified in SEM images of **type I HA** AAOs at the transition point from the galvanostatic to the potentiostatic regime for U_T values of 40, 65, and 80 V, as determined by image analysis procedures reported elsewhere,[28] had areas of 6.24, 4.32, and 5.03 μm^2, respectively.

Figure 3b shows the dependence of D_{int} and ζ_{HA} on j at $U_T = 40$ V, also determined at the transition point from the galvanostatic to the potentiostatic regime. The comparison of the full widths at half-maximum of the nearest neighbor distance distributions reveals that the pores formed at higher j values are less ordered than those formed at smaller j values. The D_{int} values of AAOs formed at $U_T = 40$ V decrease from $D_{int} = 84$ nm for $j = 25$ mA cm^{-2} to $D_{int} = 70$ nm for $j = 1000$ mA cm^{-2}. ζ_{HA} lies in the range from 2.1 to 1.75 nm V^{-1}, revealing that j is a key parameter governing D_{int} if U is kept constant.

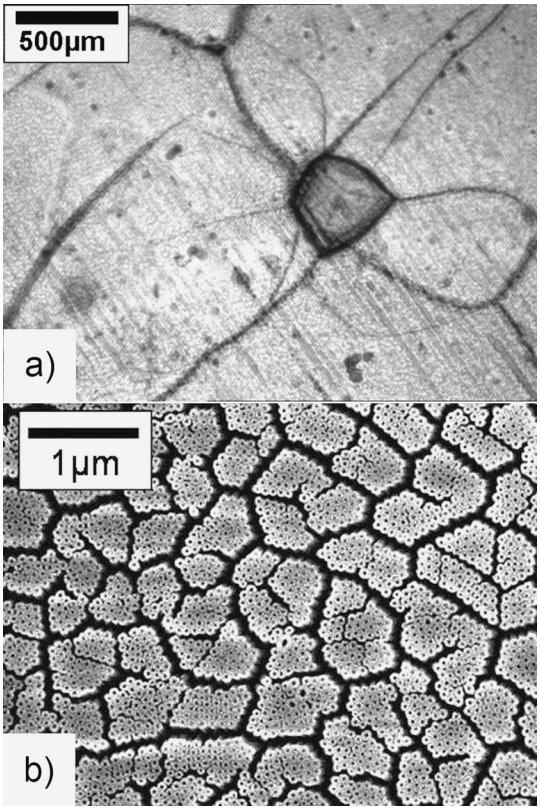

Figure 4. (a) Optical micrograph of an AAO film formed at U_T = 40 V (j = 200 mA cm^{-2}) under type I HA conditions containing macroscopic burns and cracks. (b) SEM image of a type I HA AAO film formed at U_T = 65 V (j = 200 mA cm^{-2}). Under these conditions, the pronounced formation of cracks along the cell boundaries is observed.

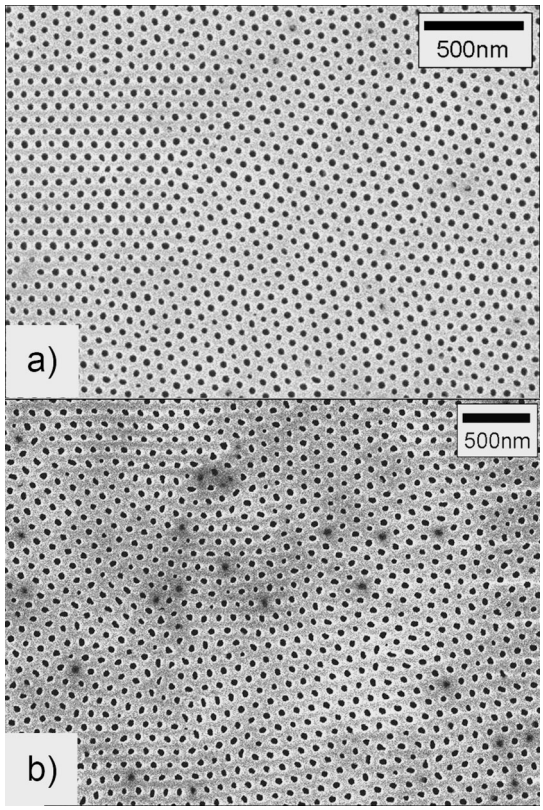

Figure 5. Representative SEM images of the undersides of AAOs formed by type II HA at (a) U_T = 40 V (j = 73 mA cm^{-2}) and (b) U_T = 65 V (j = 50 mA cm^{-2}). After the Al substrate was selectively etched, the pore bottoms were opened by ion milling.

The pore growth under **type I HA** conditions is much faster than that under MA conditions. For j = 120 mA cm^{-2} the pore depth T_p increased from 11.5 µm at U = 27 V to 40 µm at U = 32 V. At the transition from the galvanostatic mode to the potentiostatic mode at $U = U_T$ = 40 V, T_p amounted to 129 µm, and T_p reached 140 µm after further anodization under potentiostatic conditions (U_T = 40 V) for 10 min, as determined by SEM screenings of cross-sectional specimens. Moreover, the T_p value obtained at the transition from the galvanostatic to the potentiostatic regime increased from 129 µm for U_T = 40 V to 190 µm for U_T = 50 V to 230 µm for U_T = 65 V to 300 µm for U_T = 80 V. We also found a decrease of T_p along with increased values of the set current density limitation in the galvanostatic mode. For AAO formed with U_T = 40 V, at the transition from the galvanostatic to the potentiostatic regime T_p values of 320, 178, 129, and 73 µm were found for current density limitations of 25, 50, 120, and 1000 mA cm^{-2}, respectively.

AAOs prepared by **type I HA** exhibit a greenish brown to deep brown color and contain many burns and cracks discernible even with the naked eye (Figure 4a). The membranes are very brittle, and SEM investigations revealed that **type I HA** AAO may contain also cracks along cell boundaries. An example of a sample with particularly weak cell junctions leading to crack formation along the cell boundaries,[21,23,27,29] which was anodized with a U_T = 65 V and j = 200 mA cm^{-2}, is seen in Figure 4b. Only AAOs formed at U_T = 40 V with a limiting current density of $j \geq$ 750 mA cm^{-2} are colorless and transparent but show pronounced fissures along the cell boundaries too.

Chu *et al.*[21] previously suggested that the use of "aged sulfuric acid" would significantly influence **type**

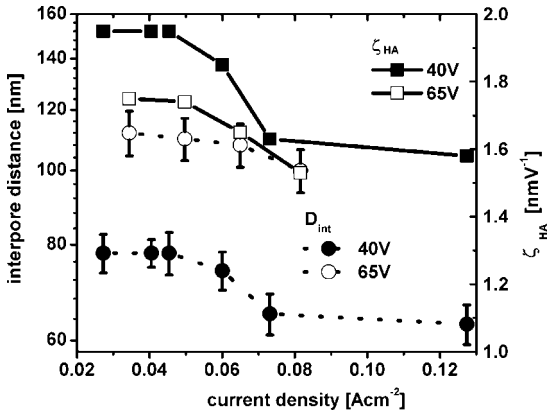

Figure 6. Dependence of D_{int} and ζ_{HA} on the current density for type II HA at U_T = 40 V and U_T = 65 V. The error bars correspond to the full widths at half-maximum of the nearest neighbor peaks in the pair distribution functions obtained from SEM images. The lines are guides for the eyes.

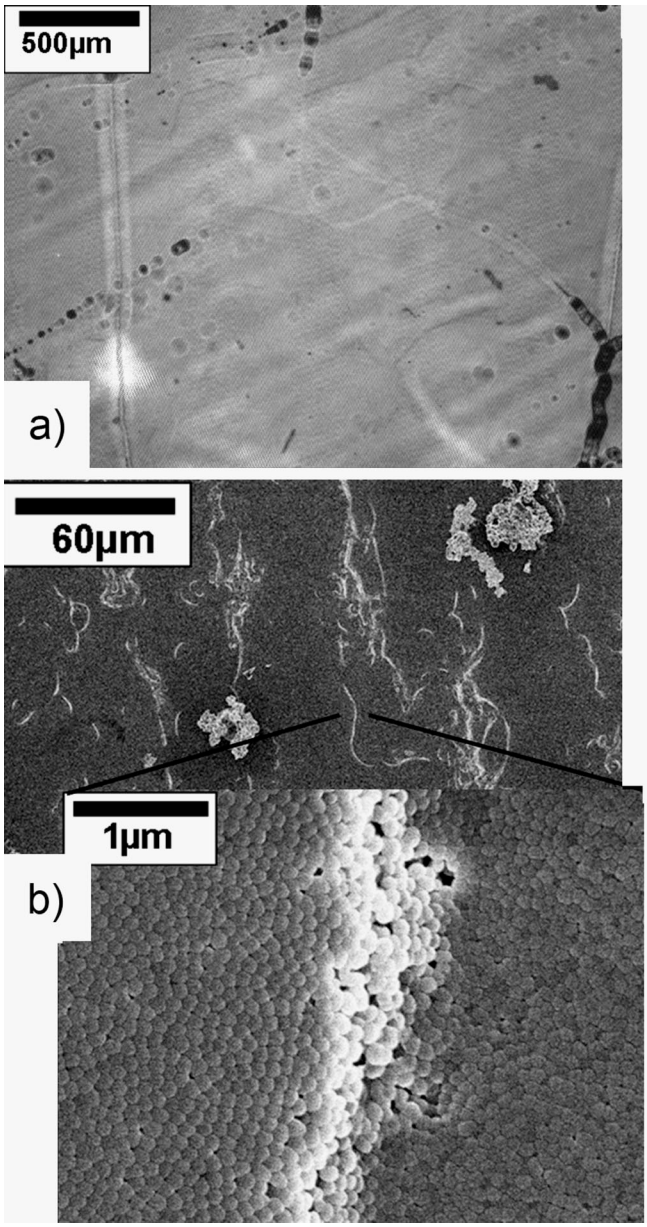

Figure 7. (a) Optical micrograph of a type II HA AAO film formed at U_T = 40 V. (b) SEM images of a type II HA AAO film formed at U_T = 65 V exhibiting plastic deformations which locally affect the pore ordering.

I HA. In order to investigate the potential impact of Al(III) species dissolved in the electrolyte solutions on **type I HA**, we performed three series of control experiments by using H_2SO_4 solutions containing different concentrations of Al(III). For this purpose, we prepared H_2SO_4 electrolyte solutions (i) by preanodizing aluminum substrates for various anodization times following the protocols reported by Chu *et al.*,[21] (ii) by dissolving AAOs prepared by H_2SO_4 anodization, and (iii) by adding $Al_2(SO_4)_3 \cdot 8H_2O$ to 10 vol % H_2SO_4. However, we could not observe any influence of the type of electrolyte solution used on **type I HA**.

Type II HA. The occurrence of structural defects such as cracks in AAOs prepared by **type I HA** is a severe drawback for their use in practical applications. In order to improve the mechanical integrity of AAOs produced by H_2SO_4-HA, we adopted a procedure previously reported for $H_2C_2O_4$-HA,[22] in which potentiostatic conditions are maintained throughout the entire process (**type II HA**, *cf.* Experimental Section). To investigate the dependence of the morphology on U_T and on j, we performed **type II HA** at U_T = 40 V and 1 °C as well as at U_T = 65 V and −1.5 °C. After U_T had been reached, we anodized the samples for different anodization times ranging from 15 to 180 min. To ensure that the anodized areas of the Al substrates are completely covered with porous alumina, the maximum value of j in the course of **type II HA** at U_T = 40 V must be larger than 127 mA cm^{-2}. For **type II HA** at U_T = 65 V, j must be kept at 380 mA cm^{-2} by sufficient cooling to avoid pronounced burning of the AAO layer. The AAO films thus obtained exhibited either a greenish light gray color for U_T = 40 V or a light gray color for U_T = 65 V. Figure 5 shows representative SEM images of the undersides of **type II HA** AAOs formed at U_T = 40 V (Figure 5a) and at U_T = 65 V (Figure 5b) after the opening of the pore bottoms.

The D_{int} value of AAOs formed under MA conditions with H_2SO_4, $H_2C_2O_4$, and H_3PO_4 solutions is proportional to the applied anodization voltage (ζ_{MA} = 2.5 nm V^{-1}).[30–32] However, under HA conditions j needs to be controlled too in order to achieve uniform pore growth. To this end, it is crucial to elucidate the dependence of D_{int} and ζ_{HA} on U_T and j in the course of **type II HA**, which is displayed in Figure 6 for U_T = 40 V and U_T = 65 V. While D_{int} increases along with U_T, ζ_{HA} decreases with increasing U_T (ζ_{HA} = 1.95 nm V^{-1} and D_{int} = 78 nm for U_T = 40 V; ζ_{HA} = 1.75 nm V^{-1} and D_{int} = 114 nm for U_T = 65 V). This implies that, in contrast to MA, the anodization voltage in the H_2SO_4-HA process is not the only parameter determining D_{int}. As evident from Figure 6, both D_{int} and ζ increase as j decreases, revealing that j is also a control parameter determining D_{int} under HA conditions. In the case of **type II HA** at U_T = 40 V, ζ_{HA} increased from 1.58 nm V^{-1} for j = 127 mA cm^{-2} ($t(U_T)$ = 15 min; $t(U_T)$ = anodization time under potentiostatic condition) to 1.95 nm V^{-1} for j = 27 mA cm^{-2} ($t(U_T)$ = 180 min). For **type II HA** at U_T = 65 V, ζ_{HA} increased from 1.53 nm V^{-1} for j = 81 mA cm^{-2} ($t(U_T)$ = 30 min) to 1.75 nm V^{-1} for j = 34 mA cm^{-2} ($t(U_T)$ = 90 min). For **type II HA** at U_T = 65 V, ordered pore growth only occurs in the current density range from 34 to 81 mA cm^{-2}. For **type II HA** at U_T = 40 V, the ordering of the pores was conserved even at j = 27 mA cm^{-2} ($t(U_T)$ = 180 min). According to our real space image analyses on SEM micrographs of **type II HA** AAOs,[28] the size of the largest domain was estimated to be 7.85 µm^2 for the sample formed at U_T = 40 V and j = 41 mA cm^{-2} ($t(U_T)$ = 120 min), and 4.85 µm^2 for the sample formed at U_T = 65 V and j = 34 mA cm^{-2} ($t(U_T)$ = 90 min). As in the case of **type I HA**, the pore

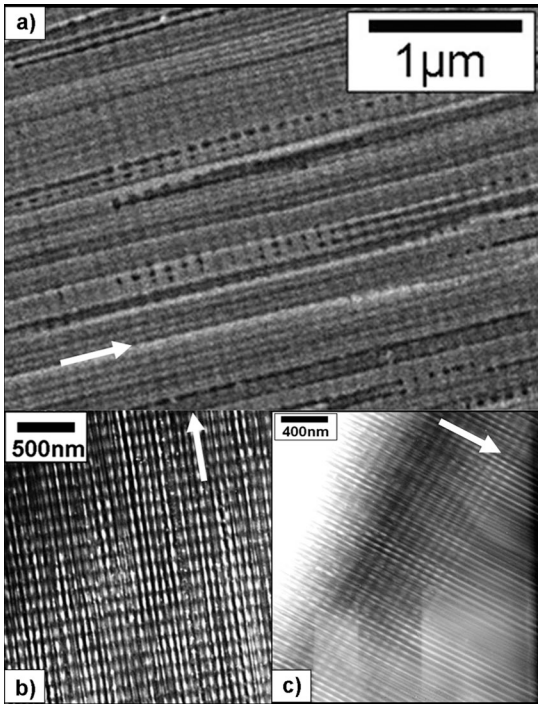

Figure 8. Electron microscopy images displaying AAO segments with modulated pores that form in the voltage range from 27 to 32 V. The white arrows indicate the growth direction of the AAOs. (a) Cross sectional SEM image of a type II HA AAO. (b) Cross sectional TEM image of type I HA (j = 200 mA cm^{-2}). (c) Cross sectional TEM image of a type I HA AAO (j = 120 mA cm^{-2}) showing the transition from pore segments with a modulated pore shape to pore segments with uniform diameter.

growth in the course of **type II HA** is significantly faster than that in conventional MA. The T_p value of **type II HA** anodized at $j = 127$ mA cm^{-2} for $t(U_T) = 15$ min amounted to 95 μm, and AAO anodized at $j = 27$ mA cm^{-2} for $t(U_T) = 180$ min had a T_p value of 360 μm. For $U_T = 65$ V, **type II HA** led to a T_p value of 155 μm if the AAOs were anodized at $j = 135$ mA cm^{-2} for $t(U_T) = 15$ min, and to a T_p value of 400 μm if the AAOs were anodized at $j = 25$ mA cm^{-2} for $t(U_T) = 120$ min. The additional dependence of the morphology of the pore arrays on j potentially poses problems with respect to the controllability of the pore growth in the course of **type II HA**. However, as obvious from Figure 6, there is a plateau where changes of j result in only negligible changes of D_{int}. Consequently, it should be possible to achieve largely uniform pore growth within certain process windows without the need to control j in addition to U_T. As a perspective on engineering of AAO membranes, it might be possible to deliberately leverage j to extend the accessible D_{int} range or to fabricate even tapered pores.

As compared to **type I HA**, we observed a strongly reduced density of cracks in AAO films obtained by **type II HA** at $U_T = 40$ V (Figure 7a). In the case of AAO films formed by **type II HA** at $U_T = 65$ V, cracks were completely absent. Also, we did not observe pore structures with distinctively weak cell junctions, unlike in the case of the **type I HA** sample shown in Figure 4b. However, AAO films formed by **type II HA** at $U_T = 65$ V exhibited macroscopic corrugations extending the entire surface of the sample, indicating the occurrence of plastic deformations in the AAO layer or in the underlying aluminum substrate (Figure 7b). We speculate that the quality and the structural integrity of the AAOs strongly depend on the local heat production during the HA process. **Type II HA** performed at $U_T \geq 75$ V was accompanied by a strong increase of j, pronounced formation of cracks and the occurrence of plastic deformations in the oxide film. It is reasonable to assume that the reaction was too exothermic for the efficient removal of the reaction heat from the reaction front.

Periodic Oscillations of the Pore Diameter. AAOs formed at $U = 27$–32 V (*cf.* voltage profiles in Figures 9 and 10) show periodic oscillations of the pore diameter with a period of about 150 nm. This phenomenon was found commonly both for **type II** (Figure 8a) and for **type I HA** (Figure 8, panels b and c). The pore shapes thus formed are reminiscent of structures that originate from the spontaneous growth of periodic fluctuations, for example, of morphologies formed by Rayleigh instabilities[33] or spinodal decomposition.[34] Yet, the mechanism leading to the formation of the oscillations is not understood. Apparently, the occurrence of the oscillations is associated with the transition from MA to HA conditions. The U profile of **type I HA** (Figure 9) exhibits a shoulder in the voltage range from 27 to 32 V where the oscillations form. If the anodization is stopped at $U < 27$ V, no pore diameter oscillations can be observed. However, if the anodization is interrupted at $U = 32$ V, modulated pores are always found. Assuming that the length of the pore segments exhibiting diameter oscillations is related to the transit time through the critical voltage range from 27 to 32 V, the length of the modulated pore segments should be inversely proportional to the limiting current. The lower the value of the limiting current density is set, the slower U increases in the galvanostatic regime and the slower the transit through the critical voltage range. For $j \geq 750$ mA cm^{-2} the shoulder peak in the **type I HA** voltage profiles vanishes along with the pore diameter oscillations, and instead a steep, nearly linear increase of the voltage occurs in the galvanostatic mode. As discussed above (Type **I HA**), these AAOs exhibit many fissures along the cell boundaries (Figure 4b).

The experimental determination of the depth of the modulated pore segments is far from being trivial. TEM analysis is limited to the area of cross-sectional specimens (*cf.* Experimental Section) that can be thinned to electron transparency, which has a maximum diameter of about 5 μm. Cross-sectional specimens for SEM investigations prepared by cleaving the AAOs commonly break along the cell boundaries so that the topology of the pores cannot be im-

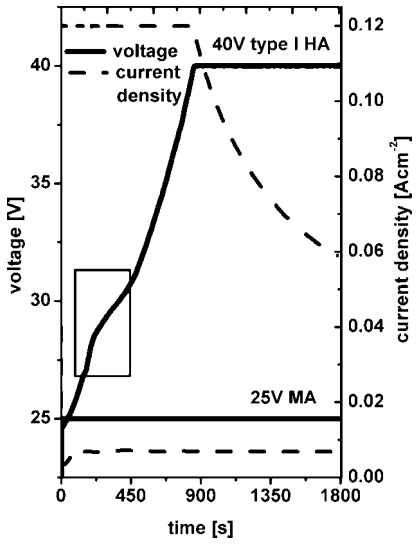

Figure 9. Current and voltage profiles of H_2SO_4-MA for U_T = 25 V and of H_2SO_4-type I HA for U_T = 40 V and j = 120 mA cm^{-2}. The voltage range where type I HA yields modulated nanopores is indicated by a rectangle.

aged. However, for a **type II HA** sample (U_T = 65 V) accidentally broken along the pore axes, the depth of the modulated pore segments was found to be 6.5 μm.

Strikingly, the formation of the oscillations at U = 27−32 V is accompanied by an intense evolution of gas bubbles over the entire surface of the samples. Previous studies revealed that oxygen is generated in barrier-type anodic oxide films formed on binary aluminum alloys.[35,36] The estimated pressure of typical bubbles with radii of around 40 nm is as high as 100 MPa, which is believed to be sufficient to cause plastic deformation of the pore walls in AAOs that have a fluid-like consistency near the reaction front. Recently, Garcia-Vergara *et al.* suggested that the stress associated with the dynamic expansion of oxygen bubbles during the anodization process causes a flow of the freshly formed alumina from the bottoms of the pores toward the cell walls.[37] We speculate that a periodic oscillation of the reaction rate could result in a periodic oscillation of the gas production rate, which in turn could lead to a periodic change of the compressive stress and a periodic modulation of the pore diameter.

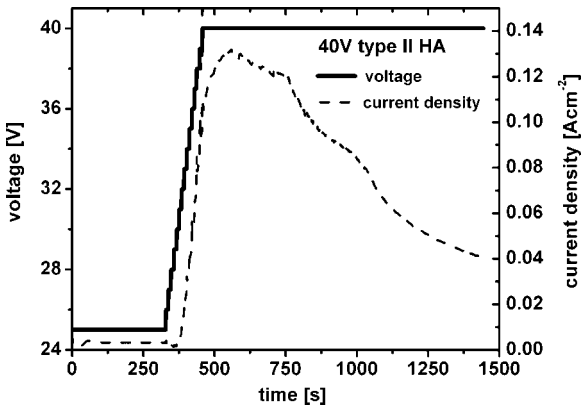

Figure 10. . Current density and voltage profiles of H_2SO_4-type II HA for U_T = 40 V.

CONCLUSIONS

The self-ordering behavior of nanoporous anodic aluminum oxide formed by hard anodization in sulfuric acid solutions was investigated. The procedures reported so far (**type I HA**) can be divided into a first stage, in which the anodization takes place under galvanostatic conditions, and a second stage, in which the anodization takes place under potentiostatic conditions. However, AAOs produced by **type I HA** have poor mechanical properties and show a pronounced tendency toward the formation of fissures along the cell boundaries. Potentiostatic conditions are maintained throughout a modified H_2SO_4-HA process (**type II HA**) that is an adaptation of a previously reported $H_2C_2O_4$-HA process.[22] **Type II HA** yields AAOs with pore depths up to several 100 μm and significantly improved mechanical properties as compared to AAOs obtained by **type I HA**. Above all, the formation of cracks along the cell boundaries, a severe drawback associated with **type I HA**, can be suppressed during **type II HA**. Real-space image analyses based on SEM micrographs revealed that efficient self-organization of the nanopores takes place in the target voltage range from U_T = 40 V to U_T = 80 V, resulting in interpore distances ranging from D_{int} = 70 nm to D_{int} = 145 nm. The ratio of D_{int} to the anodization voltage, ζ_{HA}, lies in the range from 1.75 to 2.1 nm V^{-1} and is therefore significantly smaller than that of mild anodization (ζ_{MA} = 2.5 nm V^{-1}). The interpore distance in the AAOs depends not only on the anodization voltage but also on the current density, as previously reported for $H_2C_2O_4$-HA.[22] Hence, D_{int} changes during H_2SO_4-HA. To achieve uniform pore growth, the current density has to be controlled not only under galvanostatic conditions but also under potentiostatic conditions. However, our results indicate that within certain process windows largely uniform pore growth in the course of **type II HA** can be achieved without the need of controlling the current density in addition to the anodization voltage. For applications in the fields of separation, storage, and catalysis, a tapered pore profile might be tolerable anyway. A striking finding is that the transition between mild anodization and hard anodization occurring at anodization voltages in the range from 27 to 32 V is accompanied by the formation of periodic oscillations of the pore diameter with a wavelength of the order of 150 nm. Further optimization of H_2SO_4-based hard anodization will enable the fabrication of AAOs suitable for real-life applications.

EXPERIMENTAL SECTION

Aluminum sheets (Goodfellow and Advent, 99.999%) were chemically cleaned in an aqueous mixture of 20 mL of 37 wt % HCl, 10 mL of 65 wt % HNO_3, 1 mL of 5 wt % HF, and 69 mL of H_20 at 60 °C. The sheets were then annealed for 3 h at 550 °C under nitrogen atmosphere and electrochemically polished in a 1:4 mixture of 65 wt % $HClO_4$ and 99.5 wt % ethanol under vigorous stirring. All HA experiments were carried out using an electrochemical cell[38] connected with a Keithley 2430 power supply. Both the casing and the ground plate of the cell were cooled. The anodized area was 0.785 cm^2.

In the **type I HA** experiments the anodization of surface-finished aluminum sheets was performed at set target voltages U_T ranging from 40 to 80 V at 1 °C in 1.8 M H_2SO_4 under vigorous stirring. At the early stage of **type I HA** the electrochemical oxidation of aluminum starts in the galvanostatic mode. The current density j (current divided by the sample surface) is then equivalent to the set limiting current value of the power supply and was typically set to values in the range from 25 to 1000 mA cm^{-2}. The initial rise of the voltage U is followed by a shoulder peak in the voltage profile at around 27–32 V (marked by the rectangle in Figure 9). When U reaches U_T, the anodization switches into the potentiostatic mode and j decreases exponentially. For a given U_T value the time the system is in the galvanostatic mode mainly depends on the value of the limiting current. Typical anodization profiles for **type I HA** and for H_2SO_4-based MA at $U_T = 25$ V are shown in Figure 9.

Type II HA was performed at temperatures between −1.5 and +1 °C and with U_T values in the range from 40 and 100 V. The aluminum sheets were at first anodized under MA conditions ($U_T = 25$ V in 0.3 M H_2SO_4) for 10 min to produce a thin porous alumina surface layer. Subsequently, the 0.3 M H_2SO_4 solution was replaced with a 0.03 M H_2SO_4 solution and U was gradually increased to U_T at a rate of 0.1 V s^{-1}. Thus, in contrast to **type I HA**, potentiostatic conditions were maintained during the entire process. A steady increase of j was observed along with the increase of U. When U_T was reached, j first increased to a maximum value and then decreased exponentially. A similar current–time profile was observed for $H_2C_2O_4$-HA and malonic acid-HA.[22,39] A typical anodization profile of **type II HA** is shown in Figure 10.

After the anodization, the remaining aluminum substrate was selectively removed by a wet-chemical etching step with a solution containing 3.4 g of $CuCl_2 \cdot 2H_2O$, 100 mL of 37 wt % HCl, and 100 mL of H_2O. The AAOs thus treated were investigated by SEM at an accelerating voltage of 5 kV using a JSM 6340F microscope and by TEM using a JSM 1010 machine operated at 100 kV. For the SEM studies the barrier layer covering the pore bottoms of the AAOs was removed by ion-milling (DuoMill 600, Gatan). The oxide debris generated during ion milling was washed off by immersing the membranes into 10 wt % H_3PO_4 at 20 °C for 7 min. The D_{int} values displayed in Figures 3 and 6 correspond to the maxima of the nearest neighbor peaks of the pair distribution functions obtained by real space image analysis of SEM images of the undersides of the AAO membranes.[28] The lengths of the error bars correspond to the full widths at half-maximum of the nearest neighbor peaks. For the TEM studies, cross-sectional specimens were prepared by slicing about 400 μm thick sections from samples embedded in epoxy resin with a diamond wire. The sections were ground and polished to a thickness of about 80 μm, dimple-ground, and further polished to a thickness less than 15 μm. The samples were then thinned to electron-transparency by ion etching from both sides with Ar ions (PIPS, Gatan).

Acknowledgment. K. Schwirn thanks the International Max Planck Research School for Science and Technology of Nanostructures for a scholarship. Financial support from the Volkswagen Foundation (I/80 780) and the German Federal Ministry for Education and Research (BMBF, project No. 03N8701) and support regarding TEM investigations by R. Scholz are gratefully acknowledged.

REFERENCES AND NOTES

1. Kohli, P.; Wirtz, M.; Martin, C. R. Nanotube Membrane Based Biosensors. *Electroanalysis* **2004**, *16*, 9–18.
2. Che, G. L.; Lakshmi, B. B.; Fisher, E. R.; Martin, C. R. Carbon Nanotube Membranes for Electrochemical Energy Storage and Production. *Nature* **1998**, *393*, 346–349.
3. Yamaguchi, A.; Uejo, F.; Yoda, T.; Uchida, T.; Tanamura, Y.; Yamashita, T.; Teramae, N. Self-Assembly of a Silica-Surfactant Nanocomposite in a Porous Alumina Membrane. *Nat. Mater.* **2004**, *3*, 337–341.
4. Martin, C. R. Nanomaterials - A Membrane-Based Synthetic Approach. *Science* **1994**, *266*, 1961–1966.
5. Martin, C. R. Membrane-Based Synthesis of Nanomaterials. *Chem. Mater.* **1996**, *8*, 1739–1746.
6. Lee, W.; Alexe, M.; Nielsch, K.; Gösele, U. Metal Membranes with Hierarchically Organized Nanotube Arrays. *Chem. Mater.* **2005**, *17*, 3325–3327.
7. Lee, W.; Scholz, R.; Nielsch, K.; Gösele, U. A Template-Based Electrochemical Method for the Synthesis of Multisegmented Metallic Nanotubes. *Angew. Chem., Int. Ed.* **2005**, *44*, 6050–6054.
8. Steinhart, M.; Wendorff, J. H.; Greiner, A.; Wehrspohn, R. B.; Nielsch, K.; Schilling, J.; Cho, J.; Gösele, U. Polymer Nanotubes by Wetting of Ordered Porous Templates. *Science* **2002**, *296*, 1997.
9. Steinhart, M.; Wehrspohn, R. B.; Gösele, U.; Wendorff, J. H. Nanotubes by Template Wetting: A Modular Assembly System. *Angew. Chem., Int. Ed.* **2004**, *43*, 1333–1344.
10. Kresge, C. T.; Leonowicz, M. E.; Roth, W. J.; Vartuli, J. C.; Beck, J. S. Ordered Mesoporous Molecular-Sieves Synthesized by a Liquid-Crystal Template Mechanism. *Nature* **1992**, *359*, 710–712.
11. Templin, M.; Franck, A.; DuChesne, A.; Leist, H.; Zhang, Y. M.; Ulrich, R.; Schädler, V.; Wiesner, U. Organically Modified Aluminosilicate Mesostructures from Block Copolymer Phases. *Science* **1997**, *278*, 1795–1798.
12. Zhao, D. Y.; Feng, J. L.; Huo, Q. S.; Melosh, N.; Fredrickson, G. H.; Chmelka, B. F.; Stucky, G. D. Triblock Copolymer Syntheses of Mesoporous Silica with Periodic 50 to 300 Angstrom Pores. *Science* **1998**, *279*, 548–552.
13. Masuda, H.; Fukuda, K. Ordered Metal Nanohole Arrays Made by a Two-Step Replication of Honeycomb Structures of Anodic Alumina. *Science* **1995**, *268*, 1466–1468.
14. Li, F.; Zhang, L.; Metzger, R. M. On the Growth of Highly Ordered Pores in Anodized Aluminum Oxide. *Chem. Mater.* **1998**, *10*, 2470–2480.
15. Masuda, H.; Hasegwa, F.; Ono, S. Self-Ordering of Cell Arrangement of Anodic Porous Alumina Formed in Sulfuric Acid Solution. *J. Electrochem. Soc.* **1997**, *144*, L127–L130.
16. Li, A. P.; Müller, F.; Birner, A.; Nielsch, K.; Gösele, U. Hexagonal Pore Arrays with a 50 - 420 nm Interpore Distance Formed by Self-Organization in Anodic Alumina. *J. Appl. Phys.* **1998**, *84*, 6023–6026.
17. Masuda, H.; Yada, K.; Osaka, A. Self-Ordering of Cell Configuration of Anodic Porous Alumina with Large-Size Pores in Phosphoric Acid Solution. *Jpn. J. Appl. Phys.* **1998**, *37*, L1340–L1342.
18. Shingubara, S.; Morimoto, K.; Sakaue, H.; Takahagi, T. Self-Organization of a Porous Alumina Nanohole Array Using a Sulfuric/Oxalic Acid Mixture as Electrolyte. *Electrochem. Solid-State Lett.* **2004**, *7*, E15–E17.
19. Li, Y.; Zheng, M.; Ma, L.; Shen, W. Fabrication of Highly Ordered Nanoporous Alumina Films by Stable High-Field Anodization. *Nanotechnology* **2006**, *17*, 5105–5105.
20. Ono, S.; Saito, M.; Asoh, H. Self-Ordering of Anodic Porous Alumina Formed in Organic Acid Electrolytes. *Electrochim. Acta* **2005**, *51*, 827–833.
21. Chu, S. Z.; Wada, K.; Inoue, S.; Isogai, M.; Yasumori, A. Fabrication of Ideally Ordered Nanoporous Alumina Films and Integrated Alumina Nanotubule Arrays by High-Field Anodization. *Adv. Mater.* **2005**, *17*, 2115–2119.
22. Lee, W.; Ji, R.; Gösele, U.; Nielsch, K. Fast Fabrication of Long-Range Ordered Porous Alumina Membranes by Hard Anodization. *Nat. Mater.* **2006**, *5*, 741–747.

23. Wada, K.; Shimohira, T.; Yamada, M.; Baba, N. Microstructure of Porous Anodic Oxide Films on Aluminum. *J. Mater. Sci.* **1986**, *21*, 3810–3816.
24. Csokan, P. Beiträge zur Kenntnis der Anodischen Oxydation von Aluminium Verdünnter, Kalter Schwefelsäure. *Metalloberflaeche* **1961**, *15*, B49–B53.
25. Csokan, P.; Sc., C. C. Hard anodizing: Studies of the Relation Between Anodizing Conditions and the Growth and Properties of Hard Anodic Oxide Coatings. *Electroplat. Met. Finish.* **1962**, *15*, 75–82.
26. Lichtenberger-Bajza, E.; Domony, A.; Csokan, P. Untersuchung der Struktur und Anderer Eigenschaften von durch Anodische Oxydation auf Aluminium Erzeugten Hartoxydschichten. *Werkst. Korros.* **1960**, *11*, 701–707.
27. Arrowsmith, D. J.; Clifford, A. W.; Moth, D. A. Fracture of Anodic Oxide Formed on Aluminum in Sulphuric Acid. *J. Mater. Sci. Lett.* **1986**, *5*, 921–922.
28. Hillebrand, R.; Müller, F.; Schwirn, K.; Lee, W.; Steinhart, M. Quantitative Analysis of the Grain Morphology in Self-Assembled Hexagonal Lattices. *ACS Nano*, submitted.
29. Chu, S. Z.; Wada, K.; Inoue, S.; Isoqai, M.; Katsuta, Y.; Yasumori, A. Large-Scale Fabrication of Ordered Nanoporous Alumina Films with Arbitrary Pore Intervals by Critical-Potential Anodization. *J. Electrochem. Soc.* **2006**, *153*, B384–B391.
30. O'Sullivan, J. P.; Wood, G. C. Morphology and Mechanism of Formation of Porous Anodic Films on Aluminium. *Proc. R. Soc. London, Ser. A* **1970**, *317*, 511–543.
31. Keller, F.; Hunter, M. S.; Robinson, D. L. Structural Features of Oxide Coatings on Aluminum. *J. Electrochem. Soc.* **1953**, *100*, 411–419.
32. Ebihara, K.; Takahashi, H.; Nagayama, M. Structure and Density of Anodic Oxide Films Formed on Aluminium in Oxalic Acid Solutions. *J. Met. Finish. Soc. Jpn.* **1983**, *34*, 548–554.
33. Rayleigh, L. On the Instability of Cylindrical Fluid Surfaces. *Philos. Mag.* **1892**, *23* (Serie 5), 177–180.
34. Cahn, J. W. Phase Separation by Spinodal Decomposition in Isotropic Systems. *J. Chem. Phys.* **1965**, *42*, 93.
35. Skeldon, P.; Thompson, G. E.; Wood, G. C.; Zhou, X.; Habazaki, H.; Shimizu, K. Evidence of Oxygen Bubbles Formed within Anodic Films on Aluminum-copper Alloys. *Philos. Mag. A* **1997**, *76*, 729–741.
36. Zhou, X.; Thompson, G. E.; Habazaki, H.; Paez, M. A.; Shimizu, K.; Skeldon, P.; Wood, G. C. Morphological Development of Oxygen Bubbles in Anodic Alumina. *J. Electrochem. Soc.* **2000**, *147*, 1747–1750.
37. Garcia-Vergara, S. J.; Skeldon, P.; Thompson, G. E.; Habazaki, H. Flow Model of Porous Anodic Film Growth on Aluminium. *Electrochim. Acta* **2006**, *52*, 681–687.
38. Jessensky, O. Thesis, Martin-Luther-University, Halle-Wittenberg, 1997.
39. Lee, W.; Nielsch, K.; Gösele, U. Self-Ordering Behavior of Nanoporous Anodic Aluminum Oxide (AAO) in Malonic Acid Anodization. *Nanotechnology* **2007**, *18*, 475713.